J Chem Biol (2013) 6:25–36
DOI 10.1007/s12154-012-0079-9

ORIGINAL ARTICLE

# Design and development of topoisomerase inhibitors using molecular modelling studies

**Muthu K. Kathiravan · Madhavi M. Khilare · Aparna S. Chothe · Madhuri A. Nagras**

Received: 25 April 2012 / Accepted: 24 July 2012 / Published online: 29 September 2012


**Abstract** Topoisomerase inhibitors are used as anticancer and antibacterial agents. A series of novel 2,4,6-tri-substituted pyridine derivatives reported as topoisomerase inhibitors were used for quantitative structure–activity relationship (QSAR) study. In order to understand the structural requirement of these topoisomerase inhibitors, a ligand-based pharmacophore and atom-based 3D-QSAR model have been developed. A five-point pharmacophore with one hydrophobic group (H4), four aromatic rings (R5, R6, R7 and R8) was obtained. The pharmacophore hypothesis yielded a 3D-QSAR model with good partial least-square (PLS) statistic results. The training set correlation is characterized by PLS factors ($r^2$=0.7892, SD= 0.2948, $F$=49.9, $P$=1.379). The test set correlation is characterized by PLS factors ($q^2$=0.7776, root mean squared error= 0.2764, Pearson $R$=0.8926). The docking study revealed the binding orientations of these inhibitors at active site amino acid residues of topoisomerases enzyme. The results of pharmacophore hypothesis and 3D-QSAR provided the detail structural insights as well as highlighted the important binding features of novel 2,4,6-tri-substituted pyridine derivatives and can be developed as potent topoisomerase inhibitors.

**Keywords** Pharmacophore · 3D-QSAR · Docking · Topoisomerases inhibitor · Pyridine

## Introduction

Topoisomerases are nuclear enzymes that alter the topology of DNA by transiently breaking one or two strands of DNA and controls DNA topology [1–3]. This nuclear enzyme plays an important role in the physiological function of the genome as well as DNA processes such as replication, transcription [4–6], recombination [7,8], repair [9,10], chromosome decondensation [11–14]. The topological structure of DNA is modulated by two groups of ubiquitous enzymes known as type I and type II topoisomerases [1,2]. Topoisomerases I (Topo I) are monomeric and catalyze an ATP-independent relaxation of DNA supercoils by transiently breaking and religating single-stranded DNA, whereas topoisomerases II (Topo II) are dimeric and relax supercoiled DNA through catalysis of a transient breakage of double-stranded DNA in an ATP-dependent manner [15,16].

Topoisomerase inhibitors are among the most active anticancer agents, and inhibitors of DNA gyrase are widely used as antibacterials [17]. Even drugs such as doxorubicin and mitoxantrone though used clinically are restricted due to acute toxicity and side effects associated with non-topoisomerase, secondary mechanisms of action, development of either altered topoisomerase drug resistance or multidrug resistance, etc. So, there is an overwhelming need to develop novel topoisomerase inhibitors agents with a new scaffold and different mechanisms of action distinct from existing drugs.

α-Terpyridine (Fig. 1a), a synthetic compound, showed strong cytotoxicities against several human cancer cell lines and Topo I inhibitory activities. They have the ability to form metal complexes and act as DNA/RNA binding agents [18]. α-Terpyridines are the bioisosteres of α-terthiophenes (Fig. 1b), which possess protein kinase C inhibitory activity, antitumor cytotoxicity against several human cancer cell lines as well as topoisomerase I and II inhibitory activity [18–22]. Identifying α-terpyridines as a lead, a series of pyridine substituted at 2, 4 and 6 positions with 5- or 6-memberd heteroaromatics has been reported as potent topoisomerase inhibitor against MCF-7, HeLa, DU145,HCT-15 and K562 cell lines [18–22].

M. K. Kathiravan (✉) · M. M. Khilare · A. S. Chothe · M. A. Nagras
Department of Pharmaceutical Chemistry, P. G. Research Centre, Sinhgad College of Pharmacy,
S.No.44/1, Vadgaon (Bk), Off Sinhgad Road,
Pune 411041 Maharashtra, India
e-mail: drmkkathir@gmail.com

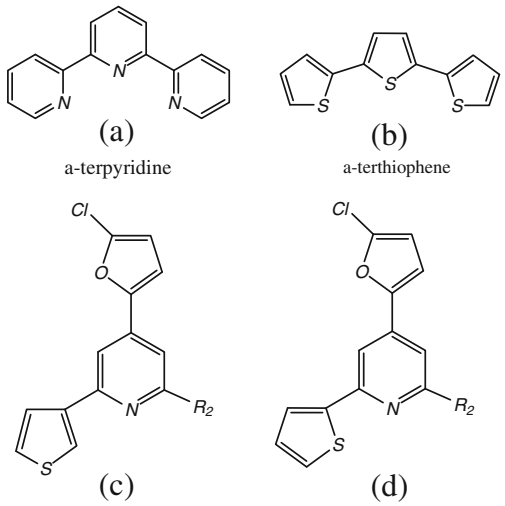


**Fig. 1** 2,4,6-Tri-substitued pyridine moiety

We herein report the molecular modelling studies on a series 2-, 4- and 6-tri-substituted pyridine (63 compounds) reported by Lee et al. as topoisomerase inhibitors [18–22]. A 3D quantitative structure–activity relationship (QSAR) study was carried out, followed by designing of new chemical entities (NCEs) from SAR study, literature survey and results of 3D QSAR studies. To gain further insights, the docking studies were performed on the designed series of NCEs with the crystal structure of topoisomerases.

## Materials and methods

### Biological data

A data set of 63 molecules belonging to 2,4,6-tri-substituted pyridine derivatives reported by Lee et al. for anticancer activity against HCT-15 was taken from the literature [18–22]. The inhibitory activities ($IC_{50}$) were converted into the corresponding PIC50 values. The structures and anticancer activity data are given in (Table 1).

### Computational details

In the present study, 3D-QSAR is performed with pharmacophore alignment, scoring engine (PHASE) and docking analysis with grid-based ligand docking with energetics (Glide) for a series of novel 2,4,6-tri-substituted pyridine derivatives as topoisomerase inhibitors. A pharmacophore modelling and 3D-QSAR study was carried out using PHASE module of Schrodinger 9.0 molecular modelling package [23–26]. All molecules were built in Maestro, and the ligands were prepared using LigPrep with the OPLS force field. Conformational space was explored through combination of Monte Carlo multiple minimum/low mode with maximum number of conformers 1,000 per structure and minimization steps 100 [27,28]. Each minimized conformer was filtered through a relative energy window of 50 kJ/mol and redundancy check of 2 Å in the heavy atom positions.

### Docking studies

Docking study was performed on Glide module from Schrodinger 9.0. The Glide algorithm approximates a systematic search of positions, orientations and conformations of the ligand in the enzyme-binding pocket via a series of hierarchical filters. Knowledge of the preferred orientation in turn may be used to predict the strength of association or binding affinity between two molecules using for example scoring functions. The shape and properties of the receptor are represented on a grid by several different sets of fields, which provide progressively more accurate scoring of the ligand pose. The binding site is defined by a rectangular box confining the translations of the mass centre of the ligand.

## Result and discussion

### Pharmacophore modelling

A set of 2,4,6-tri-substituted pyridine derivatives with $IC_{50}$ data were taken from the Lee et al. papers for the development of ligand-based pharmacophore hypothesis and atom-based 3D-QSAR model. Half maximal inhibitory concentration ($IC_{50}$) value measures the effectiveness of compound inhibition towards biological or biochemical utility. The negative logarithm of the measured $IC_{50}$ value ($pIC_{50}$) was used in this study. These 63 compounds were divided into a training set (45 compounds) and a test set (18 compounds) shown in Table 1. The training set molecules were selected in such a way that they contained information in terms of both their structural features and biological activity ranges. The most active molecules, moderately active and less active molecules were included, to spread out the range of activities [26]. In order to assess the predictive power of the model, a set of 18 compounds was arbitrarily set aside as the test set.

### Generation of common pharmacophore hypothesis

The common pharmacophore hypothesis was carried out by PHASE [27] and divided the dataset into active and inactive sets with maximum number of sites set to six and minimum to three. Final box size of pharmacophore was adjusted to 1 Å. The dataset was divided into active and inactive sets, leading to scoring protocol which provides a ranking of different hypotheses to choose most appropriate for further investigation. Inactive molecules were also scored in order

**Table 1** Observed and predicted topoisomerases activity for 2,4,6-tri-substituted pyridines

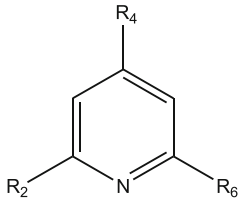


| Sr no. | $R_2$ | $R_4$ | $R_6$ | $IC_{50}$ (μm) | $pIC_{50}$ predicted | $pIC_{50}$ observed |
|---|---|---|---|---|---|---|
| 1 | 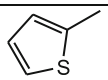 | 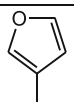 | 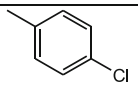 | 50.01 | 4.30 | 3.99 |
| 2 |  |  | 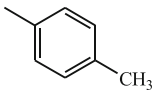 | 44.82 | 4.34 | 4.53 |
| 3[a] |  | 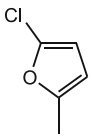 | 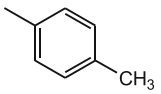 | 9.89 | 5.00 | 4.73 |
| 4 |  | 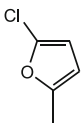 | 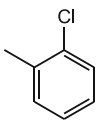 | 0.69 | 5.20 | 5.32 |
| 5 |  | 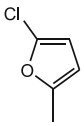 | 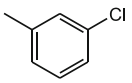 | 15.50 | 4.80 | 5.14 |
| 6 |  | 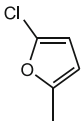 | 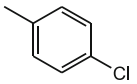 | 14.20 | 4.84 | 4.75 |
| 7 |  | 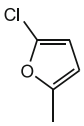 | 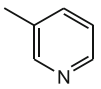 | 1.24 | 5.90 | 5.60 |
| 8 | 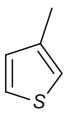 | 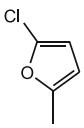 | 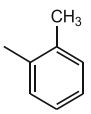 | 4.63 | 5.33 | 5.78 |
| 9 | 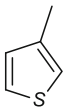 | 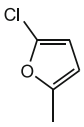 | 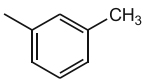 | 21.71 | 4.66 | 5.03 |

**Table 1** (continued)

| Sr no. | $R_2$ | $R_4$ | $R_6$ | $IC_{50}$ (μm) | $pIC_{50}$ predicted | $pIC_{50}$ observed |
|---|---|---|---|---|---|---|
| 10[a] | 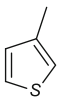 | 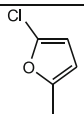 | 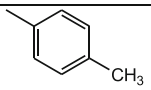 | 7.41 | 5.13 | 4.81 |
| 11[a] | 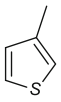 | 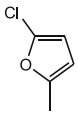 | 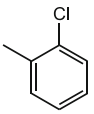 | 4.57 | 5.34 | 5.31 |
| 12 | 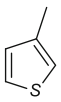 | 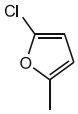 | 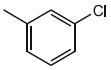 | 13.67 | 4.86 | 5.01 |
| 13[a] | 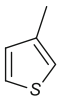 | 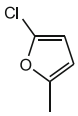 | 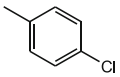 | 5.19 | 5.28 | 4.83 |
| 14 |  |  |  | 50.57 | 4.29 | 4.54 |
| 15[a] |  | 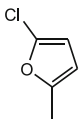 |  | 95.53 | 4.01 | 4.43 |
| 16 | 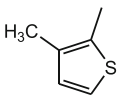 |  |  | 56.41 | 4.24 | 4.58 |
| 17 | 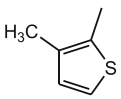 |  |  | 51.06 | 4.29 | 4.58 |
| 18 | 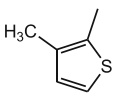 |  | 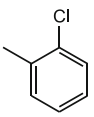 | 0.54 | 6.26 | 6.37 |
| 19 | 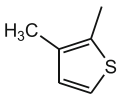 |  | 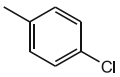 | 0.71 | 6.14 | 5.94 |
| 20 | 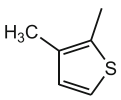 |  |  | 0.64 | 6.19 | 5.28 |
| 21 | 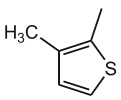 |  | 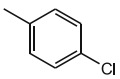 | 2.99 | 5.52 | 5.81 |
| 22 | 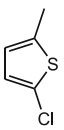 |  | 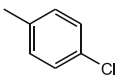 | 1.08 | 5.96 | 5.77 |

**Table 1** (continued)

| Sr no. | $R_2$ | $R_4$ | $R_6$ | $IC_{50}$ (μm) | $pIC_{50}$ predicted | $pIC_{50}$ observed |
|---|---|---|---|---|---|---|
| 23[a] | 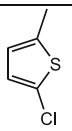 |  | 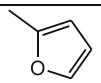 | 1.28 | 5.89 | 6.01 |
| 24[a] | 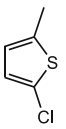 | 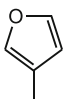 | 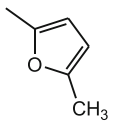 | 0.79 | 6.10 | 5.86 |
| 25[a] | 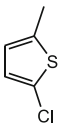 | 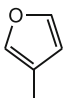 | 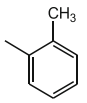 | 0.99 | 6.00 | 6.00 |
| 26[a] | 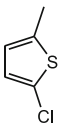 | 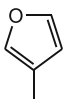 | 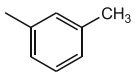 | 0.88 | 6.05 | 5.91 |
| 27 | 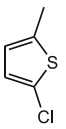 | 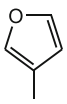 | 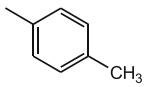 | 1.17 | 5.93 | 5.94 |
| 28[a] | 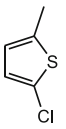 | 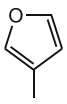 | 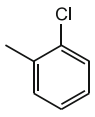 | 1.10 | 5.95 | 6.32 |
| 29 | 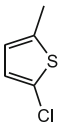 | 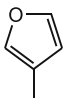 | 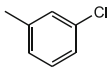 | 0.95 | 6.02 | 5.97 |
| 30 | 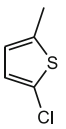 |  | 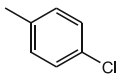 | 0.64 | 6.19 | 6.10 |
| 31 | 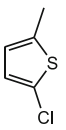 |  |  | 1.27 | 5.89 | 6.02 |
| 32 | 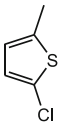 | 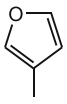 |  | 0.72 | 6.14 | 6.00 |
| 33[a] | 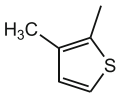 | 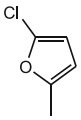 |  | 26.31 | 4.57 | 4.54 |

**Table 1** (continued)

| Sr no. | $R_2$ | $R_4$ | $R_6$ | $IC_{50}$ (μm) | $pIC_{50}$ predicted | $pIC_{50}$ observed |
|---|---|---|---|---|---|---|
| 34 | 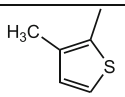 | 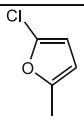 | 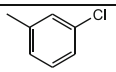 | 26.43 | 4.57 | 4.59 |
| 35 | 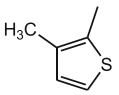 | 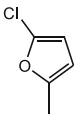 | 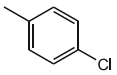 | 30.34 | 4.51 | 4.59 |
| 36 | 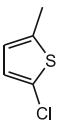 | 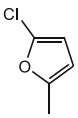 | 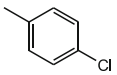 | 25.27 | 4.59 | 4.69 |
| 37[a] |  | 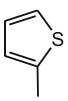 |  | 1.72 | 5.76 | 5.15 |
| 38[a] |  | 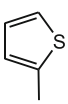 |  | 3.79 | 5.42 | 5.16 |
| 39 |  | 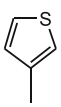 |  | 2.54 | 5.59 | 5.44 |
| 40 |  |  |  | 4.18 | 5.37 | 5.03 |
| 41 |  |  |  | 4.06 | 5.23 | 4.86 |
| 42 |  |  |  | 9.95 | 5.00 | 4.67 |
| 43 |  |  |  | 10.85 | 4.96 | 4.85 |
| 44[a] |  |  |  | 7.66 | 5.11 | 5.29 |
| 45 |  |  |  | 13.47 | 4.87 | 5.03 |
| 46 |  |  |  | 27.44 | 4.56 | 4.75 |
| 47[a] |  |  |  | 18.39 | 4.73 | 4.89 |

**Table 1** (continued)

| Sr no. | $R_2$ | $R_4$ | $R_6$ | $IC_{50}$ (μm) | $pIC_{50}$ predicted | $pIC_{50}$ observed |
|---|---|---|---|---|---|---|
| 48 | 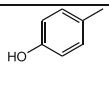 | | | 3.70 | 5.43 | 5.02 |
| 49 | 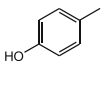 | | | 12.50 | 4.90 | 5.25 |
| 50 | 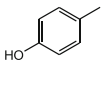 | | | 1.10 | 5.95 | 5.63 |
| 51 | 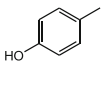 | | | 3.50 | 5.45 | 5.10 |
| 52 | 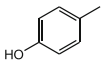 | | | 15.10 | 4.82 | 5.05 |
| 53[a] | 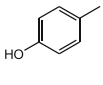 | | | 3.00 | 5.52 | 5.29 |
| 54 | | | | 2.50 | 5.60 | 5.66 |
| 55[a] | | | | 17.95 | 4.74 | 4.58 |
| 56 | | | | 14.12 | 4.85 | 4.79 |
| 57[a] | | | | 24.56 | 4.60 | 4.79 |
| 58 | | | | 13.86 | 4.85 | 5.16 |
| 59 | | | | 20.91 | 4.67 | 4.90 |
| 60 | | | | 18.39 | 4.73 | 4.90 |
| 61 | | | | 18.71 | 4.72 | 4.64 |
| 62 | | | | 5.10 | 5.29 | 5.68 |
| 63 | | | | 11.70 | 4.93 | 4.88 |

[a]Test compound

to observe the alignment of these molecules with respect to the different pharmacophore hypotheses and to select the best ones. The molecules with $pIC_{50}$ values higher than 4.9 were considered to be active, and less than 4.9 were considered to be inactive. The generated pharmacophore hypotheses were evaluated on the basis of 'Survival' and 'Survival-inactive' scores. The larger is the difference between the score of active and inactives, the better is the hypothesis at discriminating the active from inactive molecules. These common pharmacophore hypotheses were examined using a scoring function to yield the best alignment of the active ligands using an overall maximum root mean square deviation value of 1.2 Å with default options for distance tolerance. The quality of alignment was measured by a survival score, defined as:

$$S = W_{\text{site}}S_{\text{site}} + W_{\text{vec}}S_{\text{vec}} + W_{\text{vol}}S_{\text{vol}} + W_{\text{sel}}S_{\text{sel}} + W_{m\text{rew}}$$

where

| | |
|---|---|
| $W$ | weights |
| $S$ | scores |
| $S_{\text{site}}$ | alignment score |
| $S_{\text{vec}}$ | vector score |
| $S_{\text{vol}}$ | volume score |
| $S_{\text{sel}}$ | selectivity score |
| $W_{\text{vec}}$, $W_{\text{vol}}$ and $W_{\text{rew}}$ | default values of 1.0 |
| $W_{\text{site}}$ while $W_{\text{sel}}$ | default value of 0.0 |
| $W_{m\text{rew}}$ | weights defined by $m-1$ |
| $m$ | number of actives that match the hypothesis |

In atom-based QSAR, a molecule is treated as a set of overlapping van der Waals spheres. Each atom (and hence each sphere) is placed into one of six categories according to a simple set of rules: Hydrogens attached to polar atoms are classified as hydrogen bond donors (D); carbons, halogens and C–H hydrogens are classified as hydrophobic/non-polar (H); atoms with an explicit negative ionic charge are classified as negative ionic (N); atoms with an explicit positive ionic charge are classified as positive ionic (P); non-ionic atoms are classified as electron withdrawing (W) and all other types of atoms are classified as miscellaneous (X). For purposes of QSAR development, van der Waals models of the aligned training set molecules were placed in a regular grid of cubes, with each cube allotted zero or more 'bits' to account for the different types of atoms in the training set that occupy the cube. This representation gives rise to binary-valued occupation patterns that can be used as independent variables to create partial least-squares (PLS) QSAR models. Atom-based QSAR models were generated for all hypotheses using the 45-member training set using a grid spacing of 1.0 Å. The best QSAR model was validated by predicting activities of the 18 test set compounds.

**Table 2** PLS statistics of PHASE 3D-QSAR model

| Parameters | |
|---|---|
| $r^2$ | 0.7892 |
| $q^2$ | 0.7776 |
| $F$ | 49.9 |
| $P$ | 1.379 |
| RMSE | 0.2764 |
| PLS factors | 3 |
| Pearson $R$ | 0.8926 |
| SD | 0.2948 |

$r^2$ coefficient of determination, $q^2$ coefficient of determination for test set, *SD* standard deviation of regression, *RMSE* root mean squared error, *Pearson R* correlation coefficient

## Pharmacophore generation and 3D-QSAR model

The top scoring hypothesis HRRRR.44 was selected as the pharmacophore model for the present data set consisted of five features: one hydrophobic group ($H_4$), four aromatic rings (R5, R6, R7 and R8). The pharmacophore hypothesis showing distance between pharmacophoric sites is depicted in Fig. 2 and Table 2. The pharmacophore hypothesis yielded a 3D-QSAR model with good PLS statistics. The training set correlation is characterized by PLS factors ($r_2$=0.7892, SD= 0.2948, $F$=49.9, $P$=1.379). The test set correlation is characterized by PLS factors ($q^2$=0.7776, root mean squared error (RMSE)=0.2764, Pearson $R$=0.8926). Results of PLS statistics of atom-based 3D-QSAR are shown in Table 2. Graph of observed versus predicted biological activity of training, and test sets are shown in Fig. 3. The goodness of model was

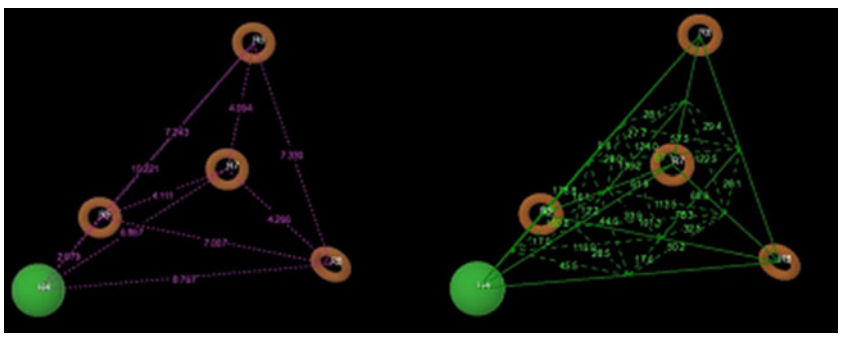

**Fig. 2** Pharmacophore hypothesis and distance between pharmacophoric sites. **a** Hypothesis with interdistances, **b** hypothesis with angles

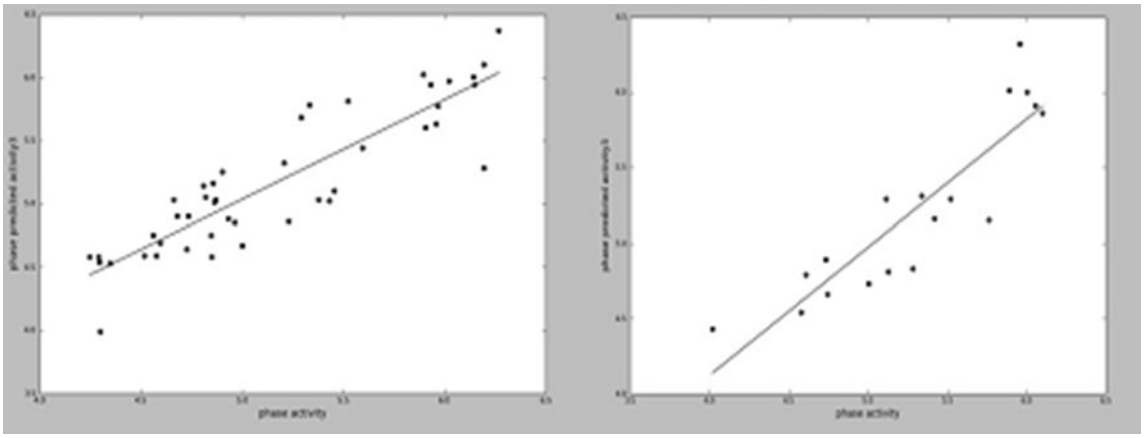

**Fig. 3** Graph of observed versus predicted biological activity of training set and test, respectively

validated by $R^2_{pred}$ ($R^2_{pred}$=0.8926) for test set. The pharmacophore site spatial distribution of HRRRR.44 model showed significant presence of hydrophobic group (H4) site in linear space of about 6 to 8 Å. Figure 4 shows the volume occlusion maps for the atom-based PHASE 3D-QSAR model (hydrophobic group and aromatic rings) represented by colour codes. These maps represent the regions of favourable and unfavourable interactions. Hydrophobic volume occlusion maps from PHASE 3D-QSAR model has shown a red-coloured region in the hypothesis indicating that an increase in formal charge in the regions is expected to improve the activity. A blue colour contour indicates decrease in formal charge to improve the activity.

The developed pharmacophore hypothesis gives information about important features for topoisomerase inhibitory activity. The cubes generated from 3D-QSAR studies highlight the structural features required for topoisomerases inhibition. These key findings from QSAR, followed by SAR study and literature data, helped us in designing a series of 50 molecules (Table 3). The designed molecules were docked into the active site of the protein along with the most potent molecules. QSAR results from Fig. 4 indicate that a five-membered ring (thienyl or furyl) is necessary at 2 and 4 positions. A phenyl ring at 6th position and hydrophobic group (2′), methyl (5′) at the 2nd position are necessary for better activity.

Docking [29–32]

The crystal structure of topoisomerase complex with 1SC7 (PDB code) was obtained from Protein Data Bank. All molecules were built within Maestro by using build, exhaustive conformational search carried out for all molecules using OPLS force field, and imposing a cutoff of allowed value of the total conformational energy compared to the lowest-energy state. Minimization cycle is for initial step size and 1.00 Å for maximum step size. In convergence criteria for the minimization, both the energy change criteria and the gradient criteria were used with default values $10^{-7}$ and 0.001 kcal/mol, respectively. Protein preparation was done by deleting all water molecules. A refined enzyme structure was used for grid file generation. All amino acids within 10 Å of the 1SC7 were included in the grid file generation.

The designed molecules are presented in Table 3 and their docking results in Table 4. The docking was performed with flexible docking method. It was validated by redocking the standard ligand (STD from Table 3) from the PDB 1SC7, and hence, the active site was validated. The ligands were docked with the active site using the ‘Extra precision’ Glide algorithm. Glide uses a hierarchical series of filters to search for possible locations of the ligand in the active-site region of the receptor. Final scoring of docked ligand is carried out on the energy-minimized poses Glide Score

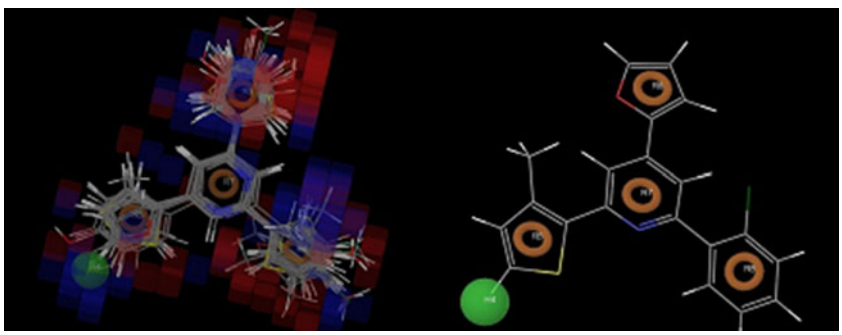

**Fig. 4** Pictorial representation of the cubes generated using the QSAR model. *Blue cubes* indicate favourable regions, while *red cubes* indicate unfavourable region for the activity

**Table 3** New chemical entity designed

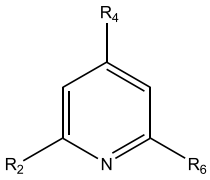


| Sr no. | $R_2$ | $R_4$ | $R_6$ | Sr no. | $R_2$ | $R_4$ | $R_6$ |
|---|---|---|---|---|---|---|---|
| *I* | 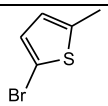 |  |  | *XVII* | 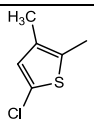 | 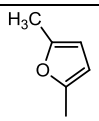 |  |
| *II* | 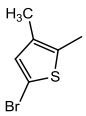 |  |  | *XIX* | 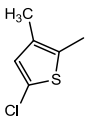 | 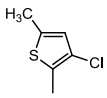 |  |
| *IV* | 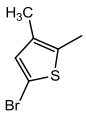 | 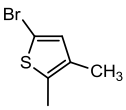 |  | *XXIII* | 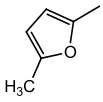 | 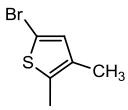 |  |
| *VII* | 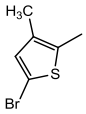 | 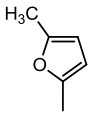 |  | *XXIV* | 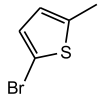 | 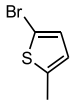 |  |
| *IX* |  |  |  | *XXVI* | 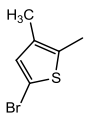 |  |  |
| *X* |  |  |  | *XXVII* |  |  |  |
| *XI* |  |  |  | *XXVIII* |  |  |  |
| *XII* |  |  |  | *XXIX* |  |  |  |
| *XIV* |  |  |  | *XXX* |  |  |  |
| *XV* |  |  |  | *XXXI* |  |  |  |
| *XVI* |  |  |  | | | | |

**Table 4** Docking scores of designed compounds

| Ligand | GScore |
|---|---|
| IV | −6.37 |
| XXVI | −5.98 |
| XII | −5.86 |
| II | −5.85 |
| XIV | −5.82 |
| XXIV | −5.81 |
| XI | −5.69 |
| XXVIII | −5.66 |
| IX | −5.57 |
| XXVIII | −5.53 |
| XVI | −5.52 |
| 10 | −5.47 |
| 27 | −5.46 |
| 7 | −5.38 |
| 29 | −5.35 |
| 19 | −5.31 |
| 23 | −5.23 |
| 30 | −5.22 |
| 15 | −5.15 |
| 1 | −5.09 |
| 31 | −5.00 |
| STD | −5.55 |

scoring function. Glide Score is based on ChemScore but includes a steric-clash term and adds buried polar terms devised by Schrödinger to penalize electrostatic mismatches.

$$\text{G Score} = 0.065 \times \text{vdW} + 0.130 \times \text{Coul} + \text{Lipo} + \text{Hbond} + \text{Metal} + \text{BuryP} + \text{RotB} + \text{Site}$$

where

| | |
|---|---|
| vdW | Van der Waal energy |
| Col | Coulomb energy |
| Lipo | lipophilic contact term |
| HBond | hydrogen-bonding term |
| Metal | metal-binding term |
| BuryP | penalty for buried polar groups |
| RotB | penalty for freezing rotatable bonds |
| Site | polar interactions at the active site |
| The Coefficients of vdW and Coul are | $a$=0.065, $b$=0.130 |

Nine compounds showed good binding affinity than the most potent molecule among the series of compounds reported as topoisomerase inhibitors (−5.55). When the second position is substituted with bromo (2′) and methyl (5′), good activity is observed. Compound 4 (Table 4) is the most active with Gscore −6.37, in which 2-bromo,5-methyl-2-thienyl are present at 2 and 4 position of pyridine. Substitution of bromo, chloro or methyl at 2′ position of 2-furyl or 2-thienyl attached at 4 position of pyridine. Substitution like bromo or chloro or fluoro, methyl shows better activity. At sixth position, phenyl or pyridine moiety is essential for activity. Compound nos. IV, XXVI, XXII, II, XIV, XXIV, XI, XVIII and IX have greater predicted activity than standard. Compound nos. XXVIII and XVI showed comparable activity with standard. Compound nos. XX, III, XIII and VI showed very less affinity than standard. Docking study of the high score moiety (compound no. IV) has binding with three amino acids ARG364, ASN352 and DC112 (Fig. 5) whereas the standard has only two amino acid interaction. The greater the amino acid binding, energy minimization takes place, increases the GScore and increases the activity. From the literature, 2,4-substitution with thienyl group exhibited strong topoisomerase I inhibitory activity. This result matches with our docking study; compound no. 4 has more predicted activity and substitution with thienyl group at 2 and 4 positions. 4-(5-Chlorofuryl)-2-(thiophen-2-yl) moiety (Fig. 1d) displayed moderate Topo I and II inhibitory showing the importance of 2-thienyl moiety.

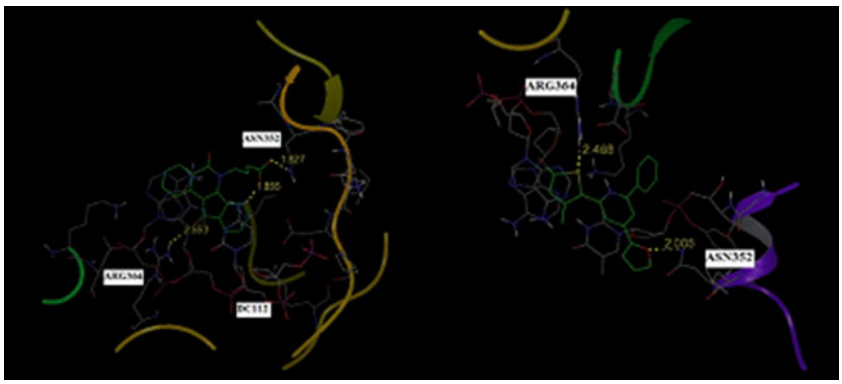


**Fig. 5** Docking of the highest scoring and standard compound with active site

## Conclusion

A highly predictive 3D-QSAR model was generated using a training set of 45 molecules which consists of five-point pharmacophore hypothesis with hydrophobic group (H4), four aromatic rings (R5, R6, R7 and R8). The developed atom-based 3D-QSAR model provides insights into the structural requirement of novel 2,4,6-tri-substituted pyridine derivatives as selective topoisomerase inhibitors. The 3D-QSAR visualization of model in the context of the structure of molecules helped in designing the molecules for docking study. The developed ligand-based pharmacophore hypothesis highlights the important binding features for novel 2,4,6-tri-substituted pyridine derivatives as topoisomerase inhibitors.

**Acknowledgments** The authors gratefully acknowledge the contributions of Prof. M. N. Navale, President, and Dr. (Mrs.) S. M. Navale, Secretary, Sinhgad Technical Education Society, Pune for constant motivation and encouragement.

## References

1. Wang JC (2002) Cellular roles of DNA topoisomerases: a molecular perspective. Nat Rev Mol Cell Biol 3:430–440
2. Wang JC (1996) DNA topoisomerases. Annu Rev Biochem 65:635–692
3. Boege F (1996) Analysis of eukaryotic DNA topoisomerases and topoisomerase-directed drug effects. Eur J Clin Biochem 34:873–888
4. Meriono A, Madden KR, Lane WS, Champoux JJ, Reinberg D (1993) DNA topoisomerase I is involved in both repression and activation of transcription. Nature 365:227–232
5. Kretzschmar M, Meisterernst M, Roeder R (1993) Identification of human DNA topoisomerase I as a cofactor for activator-dependent transcription by RNA polymerase II. Proc Natl Acad Sci USA 90:11508–11512
6. Zhang H, Wang JC, Liu LF (1988) Involvement of DNA topoisomerase I in transcription of human ribosomal RNA genes. Proc Natl Acad Sci USA 85:1060–1064
7. Lim M, Liu LF, Jacobson KD, Williams JR (1986) Induction of sister chromatid exchanges by inhibitors of topoisomerases. Cell Biol Toxicol 2:485–494
8. Shuman S (1991) Recombination mediated by vaccinia virus DNA topoisomerase I in *Escherichia coli* is sequence specific. Proc Natl Acad Sci USA 88:10104–10108
9. Yeh YC, Liu HF, Elis CA, Lu AL (1994) Mammalian topoisomerase I has base mismatch nicking activity. J Biol Chem 269:15498–15504
10. Stevnsner T, Bohr VA (1993) Studies on the role of topoisomerases in general, gene- and strand-specific DNA repair. Carcinogenesis 14:1841–1850
11. Nitiss JL (1994) Roles of DNA topoisomerases in chromosomal replication and segregation. Adv Pharmacol 29:103–134
12. Earnshaw WC, Mackay AM (1994) Role of non-histone proteins in the chromosomal events of mitosis. FASEB J 8:947–956
13. Eamshaw W, Heck M (1985) Localization of topoisomerase II in mitotic chromosomes. J Cell Biol 100:1716–1725
14. Earnshaw W, Halligan B, Cooke C, Heck M, Liu L (1985) Topoisomerase II is a structural component of mitotic chromosome scaffold. J Cell Bio 100:1706–1715
15. Holden JA (2001) DNA topoisomerases as anticancer drug targets: from the laboratory to the clinic. Curr Med Chem Anticancer Agents 1:1–25
16. Yu CX, Tse-Dinh YC, Fesik SW (1995) Solution structure of the C-terminal single-stranded DNA-binding domain of *E. coli* topoisomerase I. Biochemistry 34:7622–7628
17. Hooper DC (1998) Bacterial topoisomerases, anti-topoisomerases, and anti topoisomerase resistance. Clinical Infectious Diseases 27: S54–S63
18. Thapa P, Karki R, Choi H, Cho JH, Lee ES (2010) Synthesis of 2-(thienyl-2-yl or -3-yl)-4-furyl-6-aryl pyridine derivatives and evaluation of their topoisomerase I and II inhibitory activity, cytotoxicity, and structure–activity relationship. Bioorg Med Chem 18:2245–2254
19. Basnet A, Thapa P, Karki R, Choi H, Choi JH, Lee ES et al (2010) 2,6-Dithienyl-4-furyl pyridines: synthesis, topoisomerase I and II inhibition, cytotoxicity, structure–activity relationship, and docking study. Bioorg Med Chem Lett 20:42–47
20. Thapa P, Karki R, Thapa U, Yurngdong J, Lee ES et al (2010) 2-Thienyl-4-furyl-6-aryl pyridine derivatives: Synthesis, topoisomerase I and II inhibitory activity, cytotoxicity, and structure–activity relationship study. Bioorg Med Chem 18:377–386
21. Karki R, Thapa P, Kang MJ, Tae Cheon Jeong J, Namb M, Lee ES et al (2010) Synthesis, topoisomerase I and II inhibitory activity, cytotoxicity, and structure–activity relationship study of hydroxylated 2,4-diphenyl-6-aryl pyridines. Bioorg Med Chem 18:3066–3077
22. Basnet A, Thapa P, Karki R, Lee CS, Lee ES et al (2007) 2,4,6-Trisubstituted pyridines: synthesis, topoisomerase I and II inhibitory activity, cytotoxicity, and structure–activity relationship. Bioorg Med Chem 15:4351–4359
23. Kubinyi H (1997) QSAR and 3D QSAR in drug design part 1 methodology. Research focus 2:457–466
24. Schrödinger, LLC (2008) PHASE, version 3.0. Schrödinger, New York
25. Dixon SL, Smondyrev AM, Knoll EH, Rao SN, Shaw DE, Friesner RA (2006) PHASE: a new engine for pharmacophore perception, 3D QSAR model development, and 3D database screening: 1. Methodology and preliminary results. J Comput Aided Mol Des 20:647–671
26. Golbraikh A, Shen M, Xiao Z, Xiao YD, Lee K-H, Tropsha A (2003) Rational selection of training and test sets for the development of validated QSAR models. J Comput Aided Mol Des 17:241–253
27. Schrödinger, LLC (2008) Maestro, version 8.5. Schrödinger, New York
28. Chang G, Guida WC, Still WC (1989) An internal-coordinate Monte Carlo method for searching conformational space. J Am Chem Soc 111:4379–4386
29. Schrödinger, LLC (2008) Glide, version 5.0. Schrödinger, New York
30. FriesnerA RA, Banks JL, Murphy RB, Halgren TA, Klicic JJ, Mainz DT, Repasky MP, Knoll EH, Shelley M, Perry JK, Shaw DE, Francis P, Shenkin PS (2004) Glide: a new approach for rapid, accurate docking and scoring. 1. Method and assessment of docking accuracy. J Med Chem 47:1739–1749
31. Halgren TA, Murphy RB, Friesner RA, Beard HS, Frye LL, Pollard WT, Banks JL (2004) Glide: a new approach for rapid, accurate docking and scoring. 2. Enrichment factors in database screening. J Med Chem 47:1750–1759
32. Shah UA, Deokar HS, Kadam SS, Kulkarni VM (2010) Pharmacophore generation and atom-based 3D-QSAR of novel 2-(4-methylsulfonylphenyl)pyrimidines as COX-2 inhibitors. Mol Divers 14:559–568